An Image Processing And Neural Network Approach For Glaucoma Identification

Nidhi Pareek[1], Prof. Virendra Verma[2]

Abstract- *Glaucoma is a chronic eye disease, where a loss of vision occurs as a result of progressive optic nerve and astrocytes damage caused by high intraocular pressure (IOP). It is the second major cause of visual impairment and blindness worldwide. Early detection of the disease is critical for stopping the progression toward the complete vision loss. Due to the complex and diverse nature of disease pathology of glaucoma, its diagnosis heavily relies on the experience of glaucoma expert ophthalmologist. It is important to detect glaucoma in its early stages so that a patient's vision can be preserved. Recent advances in image processing and associated machine learning techniques have allowed to design algorithms which can automate and accurately detect glaucoma from fundus images. This paper presents an image enhancement, segmentation and denoising approach for fundus images. Further statistical features of the image have been computed which would aid the detection of glaucoma. A deep neural network is subsequently used for classification which attains an accuracy of 98%. A comparison with existing techniques show that the proposed work outperforms baseline techniques in terms of classification accuracy.*

Keywords- Automated Glaucoma Detection, Fundus Image Processing, Discrete Wavelet transform, Histogram Analysis, Feature Extraction., ANN, Classification Accuracy

I. INTRODUCTION

Glaucoma is also referred to as the silent snatcher of sight, and is the leading reason causing irreversible blindness worldwide. The risk factors and severity of sub-types of the disease may vary among races of different countries[1]. It has been found that glaucoma accounts for around 3 million cases of complete blindness and approximately 4 million cases resulting in visual impairment worldwide [2].It is apprehended that the number of people affected by any sub-type of glaucoma will exceed a staggering 110 million by 2040 [3]. Although glaucoma can be found to affect people irrespective of their age, however higher chances of occurrence (in between 1%-4%) is found among patients over the age of 40 [4]. The fundamental reason for the onset of glaucoma is the elevated level of intraocular pressure (IOP). Increased levels of IOP adversely affects the optic nerve causing irreversible damage, resulting in loss or impairment in vision depending on the magnitude of damage[5]. To save the vision of the individuals affected by glaucoma, the fundamental mechanism is to clinically reduce the levels of IOP. Clinical monotherapy or combination therapy, and in some cases surgical intervention may be required to reduce the levels of IOP to normal values[6]. While conventional medical practices have been prevalent in the diagnosis and subsequent treatment of glaucoma, recent advancements in the domain of artificial intelligence and machine learning have opened up new avenues for the early and accurate detection of glaucoma[7]. Automated computational tools can aid ophthalmologists to detect glaucoma at relatively early stages so as to minimize the damage to optic nerve and hence reduce visual impairments. Moreover, it world form the basis for a strong second opinion. It can be particularly useful in areas which lack advanced medical facilities, typically common in remote areas of low income group countries [8]. Several automated techniques have been developed and explored based on the statistical analysis of the fundus image. The basic approach is to pre-process the image to remove the effects of noise and disturbance followed by feature extraction and classification using a machine learning based classifier[10]. The machine learning based classified is trained with images of two categories viz. affected by glaucoma and unaffected with glaucoma. The classifier tries to identify the patterns in the data and hence classify any new sample of the fundus image as glaucoma positive or negative[11].

A typical illustration of glaucoma negative and glaucoma positive fundus images along with the fundus camera are illustrated in figure 1[12].

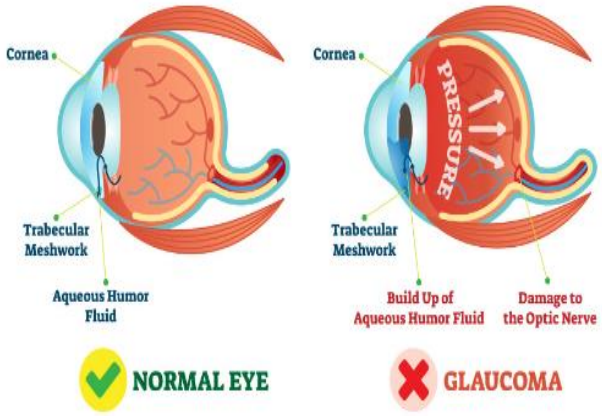

Fig. 1.Normal and Glaucoma Inflicted Eye

The fundus images obtained from fundus imaging need to be processed and analysed to extract critical features for the decision on presence or absence of glaucoma or pre-glaucoma like symptoms[13]. Due to the occurrence of noise and disturbance effects while capturing, retrieving, processing and storing the images, the final classification may be prone to errors [14]. This necessitates case sensitive noise removal and image restoration techniques which can enhance the quality of the images under interest so as to facilitate feature extraction and pattern recognition [15]. This paper presents an combined approach for image enhancement and feature extraction pertaining to fundus images which would facilitate automated detection of glaucoma.

II. MATERIALS AND METHODS

With the availability of exhaustive digital data records in the medical field coupled with the increasing processing powers of computational algorithms, automated detection of glaucoma has gained prominence. For accurate classification of glaucoma images, it is fundamentally important to pre-process the images prior to actual classification. In this paper, each of the sub-processes employed for image enhancement and subsequent feature extraction are explained in this section.

RGB to Grayscale Conversion: Typically, acquired fundus images are contain three color channels which are Red, Green and Blue (RGB channels). Analyzing high resolution RGB images requires much higher compute power as compared to analyzing images with a single intensity variable as in the case of grayscale images (with grayscale or intensity variable). The luminosity algorithm for RGB to grayscale conversion is done based on the following relation[16]:

$$I_{GS} = 0.28R + 0.5G + 0.09B \quad (1)$$

Here,

I_{GS} corresponds the pixel value of the grayscale image.

R corresponds to the red component of the pixel.

G corresponds to the green component of the pixel.

B corresponds to the blue component of the pixel.

The benefit of the approach is the conversion of the image dataset from three channels to one channel reducing the complexity of the approach.

Illumination Correction: Illumination correction corresponds to the removing the inherent illumination inconsistencies of the image due to poor or inadequate lighting conditions, variations in the reflections from the target surface due to inherent heterogeneity, variations in the angle of capture, slight movements in the position and/or orientation of the source, variations in the wavelength (monochromatic nature) of the source and inconsistencies in the characteristics of the sensing device[17]. In this approach, a Gaussian Kernel Function is used for illumination correction as it is effective in normalizing the dynamic range of the image intensities, and is mathematically expressed as:

$$G(x, y) = ke^{\frac{-(x^2+y^2)}{s^2}} \quad (2)$$

Here,

$G(x, y)$ is the Gaussian Kernel.

k represents the normalizing co-efficient.

s represents the scaling co-efficient of the kernel.

(x, y) represent the spatial co-ordinates.

The reflection co-efficient value $I_R(x, y)$ is estimated by convolving the input image and the Gaussian function in the periphery bound the contour $'C'$. The weight co-efficient w is updated throughout the contour for the number of scales $i = 1:n$. Further a linear transform to adjust the objectively captured image I and the corrected image I_C is given by:

$$I_C = \beta_1 log_e I + \beta_2 \quad (3)$$

Here,

I and I_C corresponds to the physically captured and illumination corrected images respectively.

β_1 and β_2 are correction constants.

The next process is the computation of the two-dimensional spatial correlation given by:

$$C(x,y) = \frac{I(x,y) - I_C(x,y)}{I(x,y) - I_B(x,y)} . k \quad (3)$$

Here,
C represents the correlation.
k denotes the normalizing co-efficient.
I denotes the original image
I_C denotes image correlation
I_B denotes image background

The histogram normalization is computed based on the difference in the eigen values of the original and corrected image given by:

$$|kI - I_C| \quad (4)$$

The covariance of the image can be computed as:

$$C_V = \frac{mean\ [I(x,y) - I_C(x,y)]}{|kI - I_C|} \quad (5)$$

Here,
$mean$ denotes the average operation.

The subsequent process is to add the product of the weight matrix and normalized co-variance co-efficient to the originally corrected image given by:

$$N_I = I(x,y) - I_C\{(x,y)\} + mean(w * C_V)] \quad (6)$$

Here,
N_I denotes the normalized image.
w denotes the correlation weights.

Image Inpainting: It is the restoration of the statistically deteriorated sections of the image which should spatially match the rest of the image section. Impainting can be done in several ways including recent machine learning techniques or statistical estimation and interpolation [18]. One of the major challenges in this domain is to attain low computational complexity for the system and hence an Euclidean distance based interpolation method is adopted in this section. For this purpose, the pixel correlation is computed fora patch of images wherein the inpainting is to be applied and is expressed as:

$$C_{patch} = \|P_T - P_C\|^2 \quad (7)$$

Here,
C_{patch}denotes the squared Euclidean norm for the patch.
$P_T$denotes the target patch.
$P_T$denotes the candidate patch.

In case of reconstruction, the inpainted patch pixels are weighed averages of the existing pixels satisfying the interpolation condition:

$$Z = argmin(P_T - P_C) \ll mean|P_S| \quad (8)$$

Here,
Z is the minimum interpolated difference co-efficient.
$mean|P_S|$is the average pixel magnitude of the patch.

If the above condition is not satisfied, the inpainting is to be performed based on replacing the pixel values of the patch with the sum of average and consecutive standard deviations given by:

$$\mu + \frac{\sigma^2}{(\sigma+1)^2} \quad (9)$$

Here,
μ is the average pixel values.
σ is the standard deviation.

This type of interpolation allows to inpainted the image based on the estimation of both the mean pixel values as well as the extremities based on the standard deviations. This serves as a more robust technique compared to the conventional averaging approach. To identify the patch, the radial gradient of the fundus image is to be computed given by:

$$g_r = \frac{\partial}{\partial r} \oint_{r,x_0,y_0}^{r,x_f,y_f} \frac{I(x,y)}{2\pi r} ds| \quad (10)$$

Here,
(x,y)denote image pixels
r denotes radius
g_r denotes radial gradient

Noise Removal: The next approach is the removal of the inherent noise effects in the image whose occurrence may the have following reasons[19].

1) Addition of electronic noise in the image due to the use of amplifiers in the sensing device which is also termed as white or Gaussian noise.
2) The abrupt change or spikes in the analog to digital converters sued in the circuity of the fundus image causing salt and pepper noise patterns.

3) The multiplicative noise effect due to the inconsistent gain of the adaptive gain control (AGC) circuity used for capturing or retrieving the fundus image [20].
4) The lack of pixels while capturing the image resulting in frequency mean valued interpolations in the reconstructed image causing Poisson image [21].

The removal of noise effects is fundamentally important as noisy images would result in erroneous feature extraction leading to inaccurate classification of the fundus images.

One of the most effective hyperspectral image restoration techniques is based on the sub-band decomposition of images into low pass and high pass signal values using the wavelet transform[22]. The wavelet transform, unlike the conventional Fourier methods uses non-linear and abruptly changing kernel functions which show efficacy in analysing abruptly fluctuating signals such as images[23]. The continuous and the discrete wavelet transforms are computed as[24]:

$$CWT(x,s,\delta) = s^{\frac{1}{2}} \int_{-\infty}^{\infty} x(t)\, \emptyset^*\left(\frac{t-s}{\delta}\right) dt \quad (11)$$

Where,
$s, \delta \in R$ represent the scaling (dilation) and shifting (translation) constants constrained to the condition $\delta \neq 0$.
$\emptyset^*$ is the Wavelet Family or Mother Wavelet
t is the time variable
$x(t)$ is the time domain data.

For implementing the wavelet transform on the image dataset, the sampled version of the continuous wavelet transform yields the discrete wavelet transform given by:

$$DWT(x,m,n) = \delta_0^{m\frac{-1}{2}} \sum_i x(i) \emptyset^*\left[\frac{n - is_0^m}{s_0^m}\right] \quad (12)$$

Where,
$x(i)$ is the discrete $k \times 1$ vector.
s_0^m is the discrete scaling constant.
is_0^m is the discrete shifting constant.

The discrete wavelet transform yields two distinct low and high pass values based on the number of levels of decomposition and wavelet family given by the approximate co-efficient (CA) and detailed co-efficient (CD). The approximate co-efficient values are typically the low pass values containing the maximum information content of the image while the detailed co-efficient values account for the noisy spectral part[25]. Retaining the low pass co-efficients and recursively discarding the high pass co-efficients allows to de-noise the image[26]. The choice of the wavelet family impacts the estimation of the noise gradient vector given by:

$$G_N = k\frac{\nabla I}{\nabla I_F} \quad (13)$$

The value of the second order normalizing gradient as a function of spatial co-ordinates is given by:

$$q(x,y) = \sqrt{\frac{c_1(\nabla I/I_F)^2 + c_2(\nabla^2 I/I_F)^2}{(1 + c_3(\nabla^2 I/I_F)^2}} \quad (14)$$

Here,
I denotes the original image.
I_F denotes the fused image after normalization.
G_N denotes the normalizing gradient.
∇ represents the gradient.
∇^2 represents the Laplacian.

Feature Extraction: After the pre-processing and enhancement of the image is performed, the next process is the computation of statistical and texture based features from the image dataset. In recent literature it is found that a combination of both statistical and texture features are effective for classification problems [27]. The features computed in the paper are[28]:

$$Mean = \frac{1}{N}\sum_{i,j}^{N} f_{i,j} \quad (15)$$

$$s.d. = \sqrt{\frac{1}{N}\sum_{i,j}^{N}(f_{i,j} - mean)^2} \quad (16)$$

$$v = \frac{1}{N}\sum_{i,j}^{N}(f_{i,j} - mean)^2 \quad (17)$$

$$skewness = \sqrt[3]{\frac{1}{N}\sum_{i,j}^{N}(f_{i,j} - mean)^3} \quad (18)$$

$$Kurtosis = E\left[\left(\frac{X - mean}{s.d.}\right)^4\right] \quad (19)$$

$$rms = \frac{1}{n}\sqrt{\sum_{i=1}^{n} p_i^2} \quad (20)$$

$$Energy = \sum_{i,j}^{N} |p_{i,j}|^2 \quad (21)$$

$$Contrast = \sqrt{\frac{1}{mn}\sum_{i,j}^{m,n}[X(i,j) - mean\{X(i,j)\}]^2} \quad (22)$$

$$Corr_{2D} = \sum_{i,j}^{M,N} \frac{(i-m_x)(j-m_j)P_{x,y}}{sd_x sd_y} \quad (23)$$

$$E = -P[I_{x,y}]log_2[[I_{x,y}] \quad (24)$$

$$H = \sum_{i,j}^{M,N} \frac{P_{i,j}}{1-(i-j)^2} \quad (25)$$

$$smoothness = \frac{a}{1+a} \quad (26)$$

Here,

$f_{i,j}$ corresponds to the i[th] colour component for pixel j

$mean\ (m)$ denotes the average of the statistical features.

$s.d$ denotes standard deviation

v denotes the variance

n denotes the number of pixels

p denotes the pixel value.

P denotes the probability of occurrence of pixel I w.r.t. pixel j.

$Corr_{2D}$ denotes 2-dimensional correlation

M & N denote the number pf pixels along x & y

m_x denotes mean along x

m_y denotes mean along y

sd_x denotes standard deviation along x

sd_y denotes standard deviation along y

Feature extraction serves as a serves the purpose of extracting empirical statistical information from raw data. The feature values defines in equations (15)-(26) serve as the parameters based on which any automated tool would classify a new fundus image sample as a positive or negative case of glaucoma[29].The veracity of the feature extraction process can be checked based on the correlation among the extracted features for a large dataset or a subset of the dataset. While individual image samples may exhibit divergences, yet the magnitude of such divergences in generally bound[30]. Hence, a correlation among the extracted features would testify for the correctness of the feature extraction process and its applicability for pattern recognition by any automated classifier. The image enhancement and feature extraction process can be understood using the sequence of steps described in the proposed algorithm.

Classification

While designing a machine learning algorithm for automated glaucoma detection, the following constraints should be kept in mind:

1. Typically medical image data occupies large memory (compared to text or numerical data)
2. For medical applications, the memory and processing power of the equipments would be limited. Thus the algorithm should NOT possess high computational complexity.
3. The SCG algorithm is fast and relative less computationally complex and hence is well suited for large medical image data analysis.

The scaled conjugate gradient tries to find the steepest descent vector prior to weight update in each iteration and is mathematically given by:

$$A_0 = -g_0 \quad (27)$$

Here,

A is the initial search vector for steepest gradient search

g is the actual gradient

$$w_{k+1} = w_k + \mu_k g_k \quad (28)$$

Here,

w_{k+1} is the weight of the next iteration and w_k is the weight of the present iteration

μ_k is the combination co-efficient

For any iteration k, the search vector is given by:

$$A_k = -g_k + \beta_k A_{k-1} \beta_K = \frac{(|g_{k+1}|^2 - g_{k+1}{}^T g_k)}{g_k{}^T g_k} \quad (29)$$

Here,

The customary g represents $\frac{\partial e}{\partial w}$

Proposed Algorithm:

Start.

Step. 1: Load image of interest.

Step. 2: Employ RGB-Grayscale conversion based on the relation:

$I_{GS} = 0.28R + 0.5G + 0.09B$

Step.3: Identify patch to be inpainted based on the contour 'C' enclosed by the gradient:

$$g_r = \frac{\partial}{\partial r}\oint_{r,x_0,y_0}^{r,x_f,y_f} \frac{I(x,y)}{2\pi r}\, ds|$$

Step. 4: Compute: $argmin(P_T - P_C)$

Step.5:
$if\ (argmin(P_T - P_C) \ll mean|P_S|$
Replace patch with $mean|P_S|$
$else$
Replace patch with:
$$\frac{1}{n}(\sum_{i=1}^{n}\mu + \frac{\sigma^2}{(\sigma+1)^2}$$

Step.6: For illumination correction, compute the convolution of the Gaussian kernel and the original image bounded by the contour $'C'$.
$for\ (i = 1\ to\ no.of\ scales)$
{
$$I_R(x,y) = \sum_{i=1}^{n} w[I_0(x,y) * G(x,y)]\ \forall\ (x,y)\epsilon C$$
$save\ matrix\ w_i$
}
Step.7: **Compute:**
$|kI - I_C|$
Update the normalized 2-dimensional covariance matrix as:

$$C_{V-norm} = \frac{1}{m*n}\sum_{i=1}^{m}\sum_{j=i}^{n}(x_i - x_i')(x_i - x_i')$$

Step.8: Generate fused images as:

$$I_F = wC_{V-norm}I + I_C$$

Step.9: Decide decomposition levels $'n'$ **and family of wavelet function.**

Step.10: Compute the normalizing gradient as:

$$q(x,y) = \sqrt{\frac{c_1(\nabla I/_{I_F})^2 + c_2(\nabla^2 I/_{I_F})^2}{(1 + c_3(\nabla^2 I/_{I_F})^2}}$$

Step.11: $for\ i = 1{:}n$
$retain\ C_A\ and\ discard\ C_D$

Step.12: Compute the Normal and Cumulative Histograms of the original and de-noised images, along with the histogram metrics.

Step.13: Compute Feature Distribution over the entire range of image index.

Step.14: Train the SCG based deep neural network, and truncate training on convergence.

Step.14: Test Network

Step.16: Computer Classification Accuracy
Stop.

III. RESULTS AND DISCUSSIONS

For the purpose of this study, 1000 images comprising of both positive and negative cases of glaucoma have been obtained from the Kaggle dataset [12]. The images acquired are .jpg images which three colour channels viz. R, G and B. The image enhancement and feature extraction has been performed on Matlab 2020a, with a RAM of 8GB and an i5-9300H CPU. All the images are first converted to common dimensions of $(256\ x\ 256)$ The results have been presented subsequently.

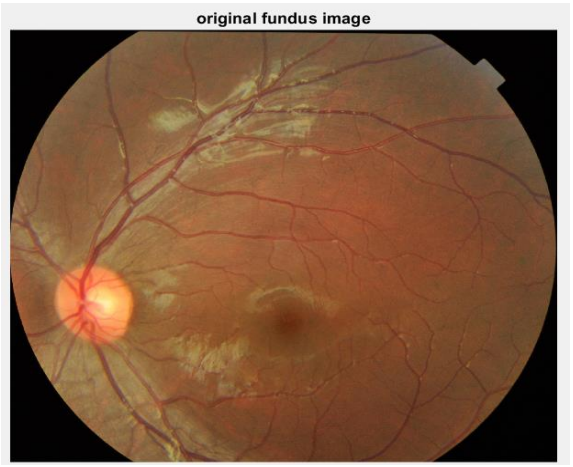

Fig.2. Original fundus image

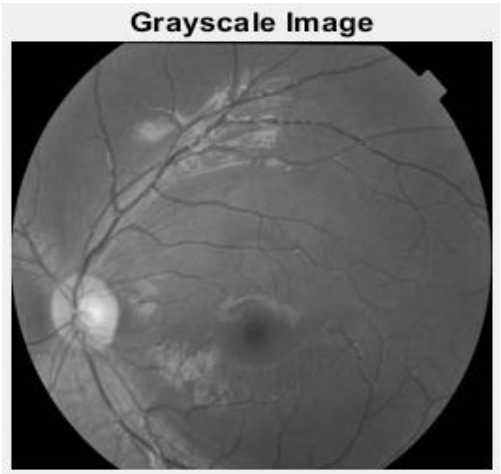

Fig.3 Grayscale Image

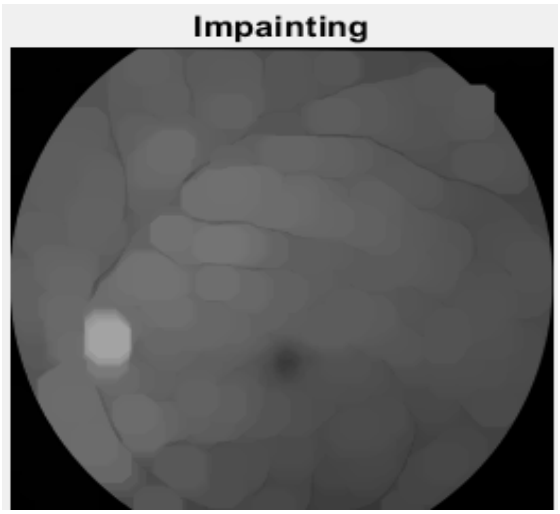

Fig.4 Applying image inpainting

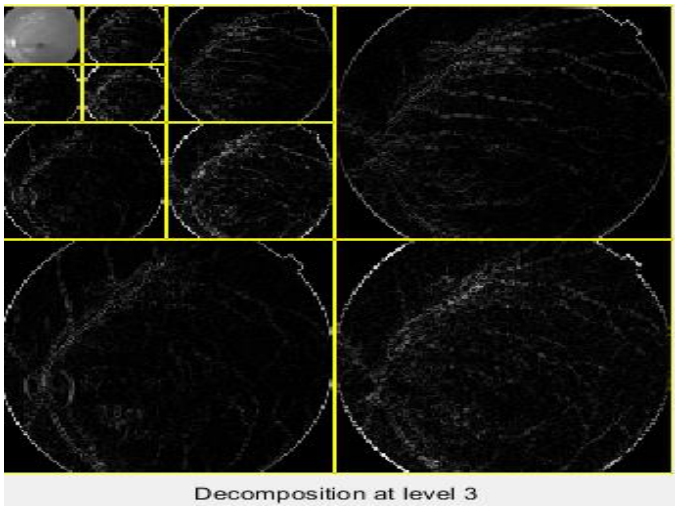

Fig.7 Haarlet decomposition at level 3.

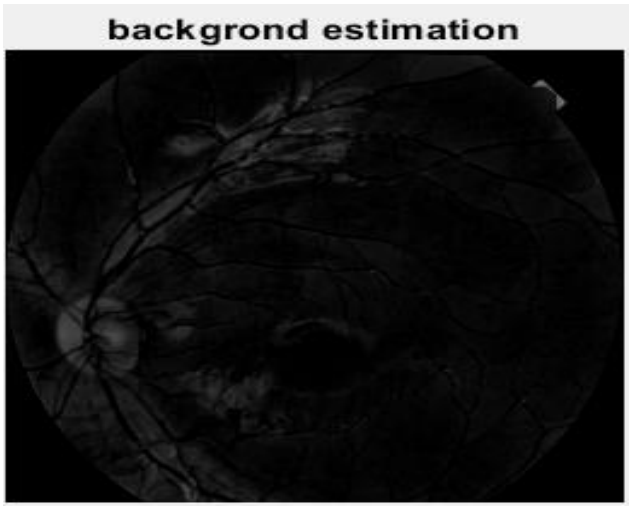

Fig.5 Background Estimation

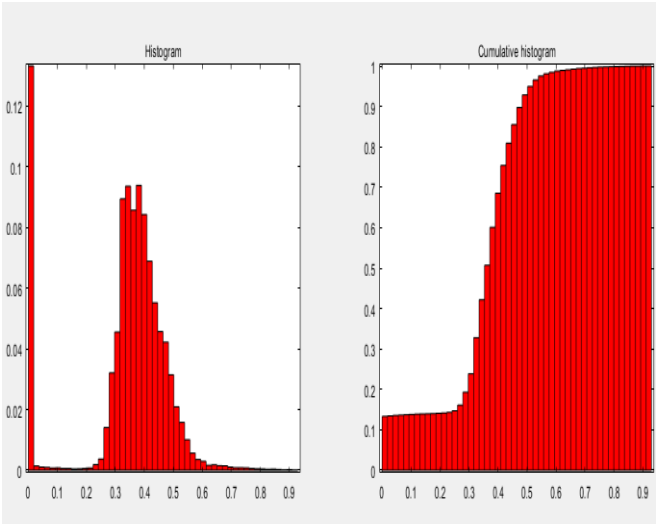

Fig.8 Histogram Analysis of original image

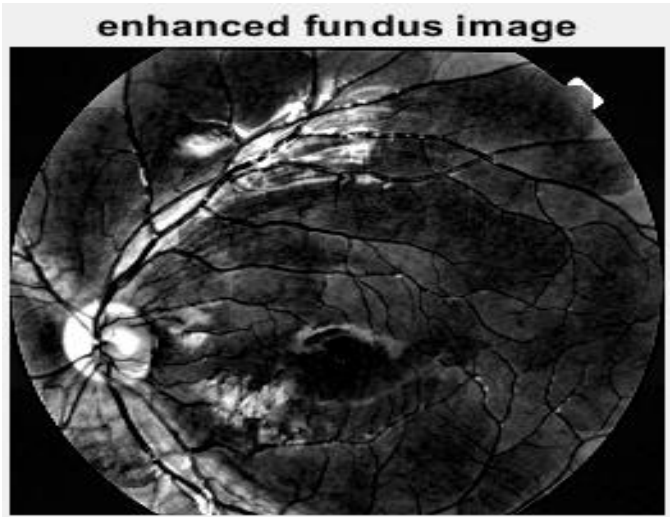

Fig.6 Enhanced image

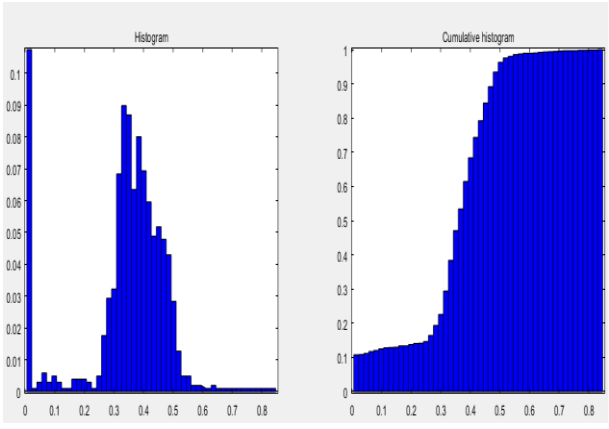

Fig.9 Histogram Analysis of approximated image

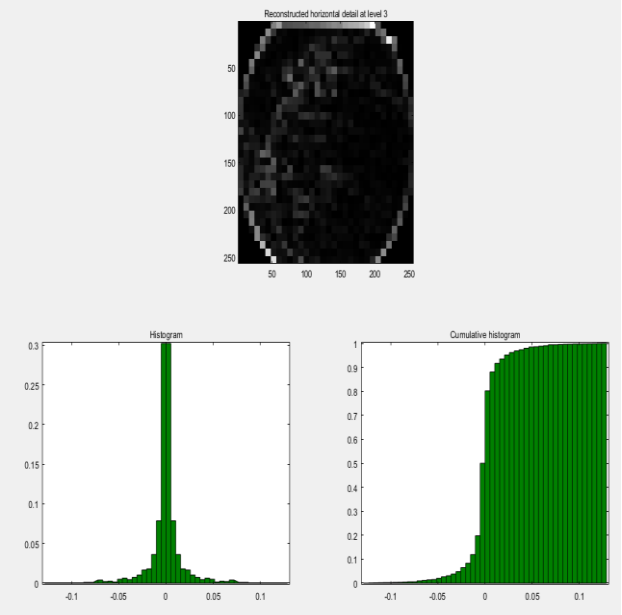

Fig.10 Histogram Analysis of detailed co-efficients of image

Table.1 Statistical parameters of the wavelet decomposition.

S.No.	Parameter	Values	Class
1.	Minimum	0	Original Image
2.	Maximum	0.9295	
3.	Mean	0.3415	
4.	Median	0.3703	
5.	Standard Deviation	0.1524	
6	Mean Absolute Deviation	0.05355	
7.	Minimum	0.002951	Approximate Co-efficient values
8.	Maximum	0.9165	
9.	Mean	0.3415	
10.	Median	0.3706	
11.	Standard Deviation	0.1511	
12.	Mean Absolute Deviation	0.05354	
13.	Minimum	-0.1592	Detailed Co-efficient values
14.	Maximum	0.1592	
15.	Mean	0	
16.	Median	0	
17.	Standard Deviation	0.01232	
18.	Mean Absolute Deviation	0.005539	

Table.2 Feature extracted

Features	Normal Fundus Image	Glaucoma Fundus Image
Contrast	0.362500000000000	0.328409090909091
Correlation	0.151836572326215	0.179081293145884
Energy	0.700218879132232	0.723267045454546
Homogeneity	0.915729166666667	0.921979166666667
Mean	0.0065264588174448 7	0.0022721221878861 3
Standard Deviation	0.106429183594269	0.106604988215597
Entropy	3.53356796596205	3.43675888527571
RMS	0.106600358177805	0.106600358177805
Variance	0.0111929089863435	0.0111892474804911
Smoothness	0.923435573787053	0.807650945366392
Kurtosis	6.63089615157184	6.70718347384146
Skewness	0.512491012022217	0.483428823467213

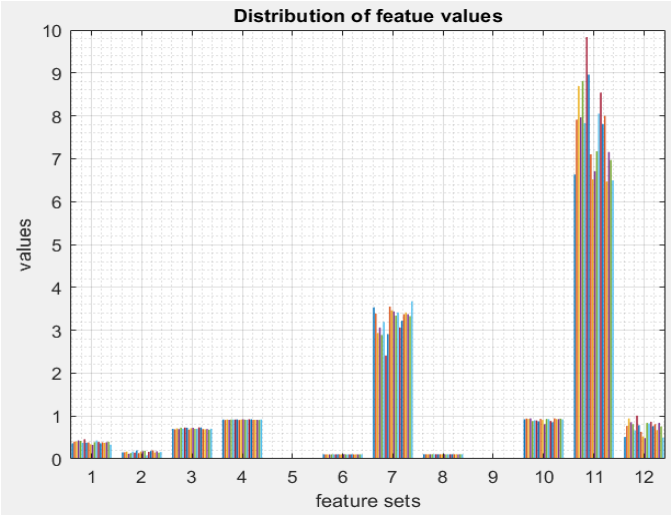

Fig. 11. Distribution of feature values

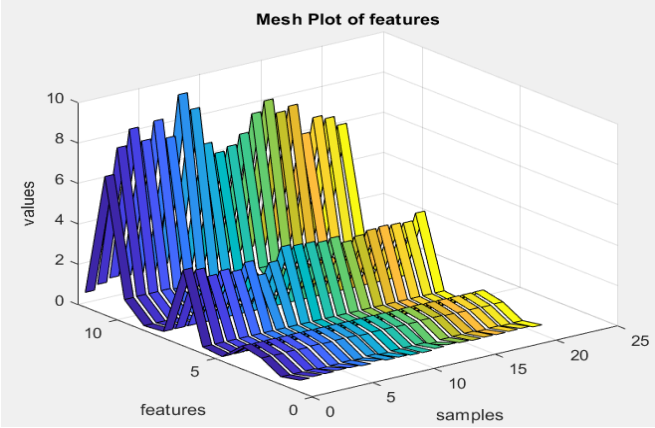

Fig.12 Mesh Plot of features

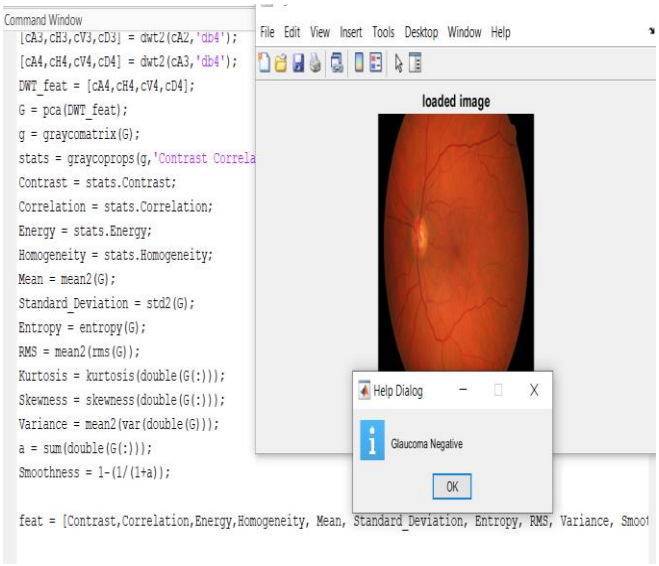

Fig. 13. Classification GUI

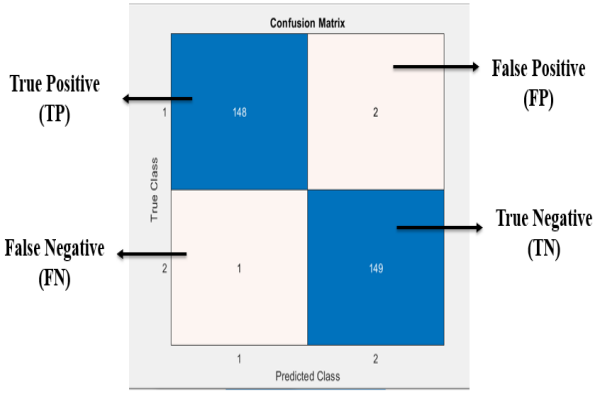

Fig. 14. Confusion Matrix

Figure 2 depicts a sample fundus image which has been used for pre-processing and image enhancement followed by feature extraction. Figure 3 depicts the image after grayscale version of the image depicted in figure 2. Figure 4 depicts the inpained image with removal of the veins and the optic nerve. The inpainting has been performed subsequent to the detection of the region of interest based on the computation of the radial gradient defined in equation (10). Figure 5 depicts the background hue, saturation, values (HSV) estimation for the fundus image. The estimation of the HSV is helpful for image quality assessment (IQA) and facilitates the image enhancement process [31]. Figure 6 depicts the enhanced image after background normalization. The background normalization process helps to clearly identify the region under interest and further feature extraction. Figure 7 depicts the haarlet decomposition of the image at level 3. The choice of the haar wavelet family has been made due to the efficacy of the haarlet corresponding to image analysis. Sudden changes and spikes in image pixel values are filtered out using the 3rd level decomposition. In the process, the approximate co-efficients are retained while discarding the detailed co-efficient of each level of decomposition. This allows the retaining maximum image information while discarding the noisy part of the image. The wavelet decomposition has been truncated to three levels to limit the system complexity. Increasing the decomposition levels beyond 5 has not shown significant improvement in image resolution based on the histogram analysis [32]. The effectiveness of the recursive wavelet decomposition has been carried out based on the histogram analysis of the original and wavelet- processed images. Figure 8 depicts the normal and cumulative histogram of the original image. The normal and cumulative histograms clearly render the statistical features of the image in the transform domain (DWT-domain). Six critical statistical features in the transform domain have been chosen in this case for the analysis which are maximum value, minimum value, mean value,median, standard deviation and mean absolute deviation. Figure 9 depicts the normal and cumulative histograms of the approximated image after retaining approximate co-efficents.Figure 10 depicts the normal and cumulative histograms of the detailed or noisy image after retaining detailed co-efficents.The statistical co-efficients of the data are tabulated in table 1.

From table 1, it can be clearly seen detailed co-efficient values however tend to deviate from the actual data stream as the number of levels increase. This clearly indicates that if the approximate co-efficient values are retained and the detailed coefficient values are discarded, then the amount of local variations and noise can be removed. The wavelet transform can be used to maintain monotonicity in local intervals so as to make the training more effective for a classifier.The above argument indicates that the wavelet decomposition for feature extraction can enhance the accuracy of prediction and also increase the regression for large data sets.As an illustration, two separate fundus images have been analysed using the proposed algorithm and their features have

been tabulated in table 2. It can be observed that the statistical feature values have identical values for both positive and negative cases of glaucoma, which necessitates the use of an accurate classifier.Figure 11 depicts the distribution of the feature values of the images which implies that the features depict good correlation.Figure 12 depicts the mesh plot of the features. The plot can be used to visualize the variation in the feature values. A correlation among the distribution of the feature values can be seen from figures 11 and 12 which imply coherence in the results. Figure 13 depicts the GUI designed for the classification. Figure 13 depicts the confusion matrix. The classification accuracy is computed as:

$$Ac = \frac{TP + TN}{TP + TN + FP + FN} = \frac{Correct\ Decisions}{Total\ Decisions}$$

$$Accuracy = \frac{148 + 149}{148 + 149 + 2 + 1} = 98.5\%$$

A comparison with Nayak et al. [31] (accuracy of 97.2%) and Wu et al. [32] (accuracy of 85%) clearly indicates that the proposed work outperforms the existing baseline techniques in terms of classification accuracy.

IV. CONCLUSION

It can be concluded from the previous discussions that it is necessary to design accurate automated tools for detection of glaucoma to inhibit the progression of the disease resulting in visual impairments and blindness. The design of automated systems, however face the challenge of the raw data being prone to noise and disturbance effects while capturing, retrieval and sharing. Moreover, the statistical features of the raw data for both positive and negative cases of glaucoma show similarity making automated accurate classification challenging. This paper presents an algorithm which first pre-processes the raw images to correct illumination inconsistencies followed by a recursive discrete wavelet transform based approach for noise removal. Subsequently, a feature extraction mechanism is proposed which is capable of computing both texture and statistical features from the images. The results show that the proposed approach attains both noise removal and coherence in feature extraction from the fundus images and serves a critical tool for accurate and automated glaucoma detection. The proposed approach presents an approach comprising of statistical feature selection and probabilistic neural network. The accuracy achieved by the proposed technique is 98.5% which is significantly higher than the existing approach.

REFERENCES

[1] Tham Y, Li X, Wong T, Quigley H, Aung T, Global prevalence of glaucoma and projections of glaucoma burden through 2040: a systematic review and meta-analysis, *Ophthalmology, Elsevier* 2014; **170** (11): 2081-2090

[2] Zaman F, Gieser S, Schwartz G, Swan C, A multicenter, open-label study of netarsudil for the reduction of elevated intraocular pressure in patients with open-angle glaucoma or ocular hypertension in a real-world setting, Current Medical Research and Opinion, *Taylor and Francis*, 2021, **37**(6): 1011-1020.

[3] Denis P, Duch S, Chen E, Klyve P, European real-world data about the use of a new delivery system containing a preservative-free multi-dose glaucoma treatment, *European Journal of Ophthalmology, SAGE Publication* 2021,**31**(3): 1056–1063.

[4] Erb, C., Gast, U, Schremmer, D. German register for glaucoma patients with dry eye. I. Basic outcome with respect to dry eye. *Graefe's Archive for Clinical and Experimental Ophthalmology, Springer* 2008, **246**:1593–1601.

[5] Safdel, A., Hassani, K. Fluid–structure interaction analysis of alteration of the intraocular pressure on the optic nerve head in glaucoma. *Journal of Optics, Springer* 2021, **50:**523–528.

[6] Schwartz G, Patel A, Naik R, Lunacsek O, Characteristics and treatment patterns of newly diagnosed open-angle glaucoma patients in the United States: an administrative database analysis, *Ophthalmology Glaucoma, Elsevier* 2021, **4**(2): 117-125.

[7] Asaoka R, Murata H, Iwase A, Araie M, Detecting preperimetric glaucoma with standard automated perimetry using a deep learning classifier, *Ophthalmology, Elsevier* 2016, **123**(9):1974-1980.

[8] Suvarna H, Patil G, Automatic Glaucoma Detection Using CDR on Morphology and Hough Based Technique, *2018 International Conference on Electrical, Electronics, Communication, Computer, and Optimization Techniques (ICEECCOT)*, 2018, 954-96.

[9] Fu H., Cheng J., Xu Y., Liu J. Glaucoma Detection Based on Deep Learning Network in Fundus Image. In: Lu L., Wang X., Carneiro G., Yang L. (eds) Deep Learning and Convolutional Neural Networks for Medical Imaging and Clinical Informatics. *Advances in Computer Vision and Pattern Recognition. Springer*, 2019: 119-137

[10] Salam A, Khalil T., Akram, M. et al. Automated detection of glaucoma using structural and non structural features. *Springer Plus*, 2016, **5**:1519.

[11] Ștefan A, Paraschiv E, Ovreiu S Ovreiu E, A Review of Glaucoma Detection from Digital Fundus Images using Machine Learning Techniques, *International Conference on e-Health and Bioengineering (EHB)*, 2020:1-4.

[12] Glaocoma Image Dataset, accessed from: https://www.kaggle.com/linchundan/fundusimage1000

[13] Lim C, Lee C, Huang F, Huang J, Risk of Glaucoma in Patients Receiving Hemodialysis and Peritoneal Dialysis: A Nationwide Population-Based Cohort Study, *International Journal of Environmental Research and Public Health, MDPI*, 2020, **17**(18):6774.

[14] Sarkar D., Das S. Automated Glaucoma Detection of Medical Image Using Biogeography Based Optimization. In: Bhattacharya I., Chakrabarti S., Reehal H., Lakshminarayanan V. (eds) *Advances in Optical Science and Engineering. Proceedings in Physics Springer*, 2017, **194:** 381-388.

[15] Vijapur A., Kunte, R. Sensitized Glaucoma Detection Using a Unique Template Based Correlation Filter and Undecimated Isotropic Wavelet Transform. *Journal of Medical and Biological Engineering, Springer* 2017, **37**:365–373.

[16] Kumar K, Mishra R, Nandan D, Efficient Hardware of RGB to Gray Conversion Realized on FPGA and ASIC, *Procedia Computer Science, Elsevier* 2020, **171**(2008):2015.

[17] Cheng, K., Yu, Y., Zhou, H., GPU fast restoration of non-uniform illumination images. *Journal of Real-Time Image Processing, Springer* 2021, **18**:75–83.

[18] Elharrouss, O., Almaadeed, N., Al-Maadeed, S. Image Inpainting: A Review, *Neural Process Letters, Springer* 2020, **51**:2007–2028.

[19] Khmag, A., Ramli, A, Al-haddad S, Natural image noise level estimation based on local statistics for blind noise reduction. *The Visual Computer, Springer* 2018, **34**: 575–587.

[20] Choi H, Jeong J, Speckle noise reduction in ultrasound images using SRAD and guided filter, *2018 International Workshop on Advanced Image Technology (IWAIT),IEEE, 2018*:1-4.

[21] Dytso A, Vincent Poor H, Estimation in Poisson Noise: Properties of the Conditional Mean Estimator, *IEEE Transactions on Information Theory*, 2020, **66**(7) :4304-4323.

[22] Khmag, A., Haddad S., Ramlee R,. Natural image noise removal using non local means and hidden Markov models in stationary wavelet transform domain. *Multimedia Tools and Applications, Springer* 2018, **77**:20065–20086.

[23] Qin L, Wang Z, Guan Q, Guo X, Wang G, Variational Bayesian image restoration with multi-structured model of wavelet transform coefficients, *Signal Processing: Image Communication, Elsevier*, **72**: 1-8.

[24] He, L., Wang, Y., Xiang, Z. Wavelet frame-based image restoration using sparsity, nonlocal, and support prior of frame coefficients. *The Visual Computer, Springer* 2019, **35**: 151–174 (2019).

[25] Kimlyk M, Umnyashkin S, Image denoising using discrete wavelet transform and edge information, *2018 IEEE Conference of Russian Young Researchers in Electrical and Electronic Engineering (EIConRus)*, 2018: 1823-1825.

[26] Singh L., Janghel R. Image Denoising Techniques: A Brief Survey. In: Yadav N., Yadav A., Bansal J., Deep K., Kim J. (eds) Harmony Search and Nature Inspired Optimization Algorithms. *Advances in Intelligent Systems and Computing, Springer* 2019, **741:** 731-740.

[27] Pal B., Bhateja V., Johri A., Pal D., Satapathy S. Glaucoma Detection Using Morphological Filters and GLCM Features. In: Satapathy S.C., Bhateja V., Favorskaya M.N., Adilakshmi T. (eds) Smart Computing Techniques and Applications. *Smart Innovation, Systems and Technologies, Springer* 2021, **224:** 627-635.

[28] Srivastava, D., Rajitha, B., Agarwal, S. Pattern-based image retrieval using GLCM. *Neural Computing and Applications, Springer* 2020, **32:** 10819–10832